THE SCALED THERMAL EXPLOSION EXPERIMENT

J.F. Wardell, J. L. Maienschein
Lawrence Livermore National Laboratory
P.O. Box 808, L-282
Livermore, CA 94550

We have developed the Scaled Thermal Explosion Experiment (STEX) to provide a database of reaction violence from thermal explosion for explosives of interest. Such data are needed to develop, calibrate, and validate predictive capability for thermal explosions using simulation computer codes. A cylinder of explosive 25, 50 or 100 mm in diameter, is confined in a steel cylinder with heavy end caps, and heated under controlled conditions until reaction. Reaction violence is quantified through non-contact micro-power impulse radar measurements of the cylinder wall velocity and by strain gauge data at reaction onset. Here we describe the test concept, design and diagnostic recording, and report results with HMX- and RDX-based energetic materials.

INTRODUCTION

Development of an understanding of and predictive capability for the hazards involved in thermal explosions of energetic materials exposed to high temperatures such as fires requires that we understand the fundamental reactions of energetic materials exposed to thermal stimuli. We also must quantify the reaction violence that result from these fundamental reactions. With quantified violence data, we can validate computational tools currently being developed and applied to cookoff problems.[1] The Scaled Thermal Explosion Experiment (STEX) is designed to quantify the violence of thermal explosions under carefully controlled conditions, and to provide a database which we can use to validate predictive codes and models. The use of the data from this experiment is complemented by separate measurements of fundamental reaction kinetics, deflagration behavior, and thermal and mechanical properties as reported in our companion paper.[2]

Previous experimental studies of reaction violence have been limited by the available diagnostics to quantify the violence. Many thermal explosion experiments done to date have been screening tests to determine qualitative violence, typically by observing number and size of fragments. Further, the initial and boundary conditions are often not well known, since screening experiments are generally low-cost, which makes it difficult to tightly control the external and internal conditions. Other experiments have been run at a very small scale. These can be carefully designed to emphasize a particular aspect of thermal reaction, but are difficult to extrapolate to scales more representative of actual systems. We developed the STEX test to address the lack of quantitative data on thermal reaction violence. Here we discuss the design of the STEX test, and present results with HMX- and RDX-based energetic materials. We also report on a method used to estimate the percent of detonation energy represented by the thermal explosion, which provides a useful comparison of different explosives. The work reported here represents progress towards our goal to provide a database of violence of thermal explosions for materials of interest under well controlled conditions to support the development of a predictive capability of thermal explosion violence.

EXPERIMENTAL CONCEPT

The STEX test was developed with the following goals: uniform heating for well-defined boundary conditions; well-defined physical confinement; pre-determined reaction location away from end effects; a range of physical scales; quantitative measurements of reaction violence; and a design to allow accurate simulations of the system while avoiding physical features that are difficult to model. To this end, we devised a cylindrical test, shown in Figure 1, where the reaction initiates in the axially central region of the cylinder (radial location depends on heating rate). Confinement is provided by a steel wall and end caps with known

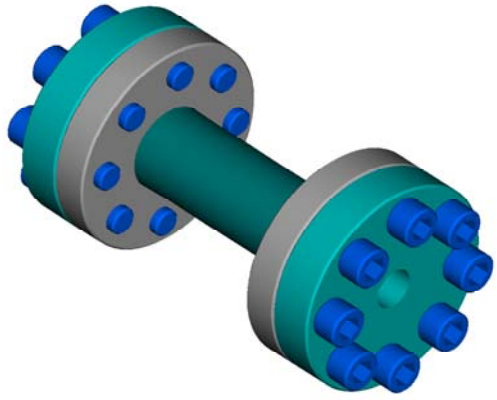

FIGURE 1. DESIGNER'S RENDITION OF THE 50.8MM STEX VESSEL. NOTE THE VESSEL TUBE, BRAZED FLANGES THICK END CAPS AND LARGE BOLTS.

mechanical properties that are not very sensitive to temperature. Confinement levels are 50, 100, or 200 MPa, set by selecting the thickness of the cylinder wall. For 50.8 mm diameter, 203 mm length, the respective wall thickness were 1.02, 2.03, 4.06 mm. We use a constant length to diameter ratio of 4:1.

EXPERIMENTAL DESIGN

The design of the STEX vessel is shown in Figure 2. The cylindrical vessel is made of 4130 steel hardened to Rockwell 32C. A flange (152 mm diameter, 25.4 mm thick) is brazed onto each end of the vessel, and sealed with an end cap (152 mm diameter, 28.4 mm thick) using a metal O-ring and several heavy bolts.. The metal O-ring, from Parker-Hannifin Corporation, is a hollow torus made from X750 Inconel with a free height diameter of 3.2 mm, a wall thickness of 0.51 mm, and an overall diameter scaled to fit the diameter of the vessel and end flanges. The O-ring is internally vented so that internal pressure assists in achieving a leak-free seal at high pressures. In developing this design, we extensively analyzed the mechanical response of the system to anticipated stresses and ensured that the weak point in the system was the cylinder wall and not the end caps.

External temperature is controlled by three RTDs (one for cylindrical vessel and one for each end cap), and monitored by twelve additional RTDs placed at locations at 60° intervals 1/4, 1/2, and 3/4 of the way up the vessel wall; these RTDs are calibrated to ± 0.1°C. The RTDs are attached to the outside diameter of the vessel wall with a high temperature two-part epoxy system. An internal thermocouple sheath is placed on the axis of the cylinder, in the explosive, with thermocouples at each end of the vessel and at 1/4, 1/2, and 3/4 height locations. The sheath is fabricated from type 304 stainless steel (1.6 mm OD, 0.4 mm wall thickness) with a welded end plug. The sheath was designed to withstand 200 MPa pressure, which is the maximum it should see before the final explosion. Type K thermocouples calibrated to ± 0.5°C are inserted into the sheath to measure the temperature at the positions given above.

There are two types of strain gauges used on the STEX vessel: the 350 ohm WK series gauge with a strain range of ±1.5% and the 120 ohm EP series gauge having a strain range of 20%. These gauges are installed in a full-bridge configuration. The adhesive used (M-bond 610) is rated to about 3% strain, and therefore limits the range of our strain data. The strain gauges are used to measure both axial and hoop strain. One gauge of each type is used to measure axial strain, and another of each type is used for hoop strain.

In the latest experiments, a pressure transducer is installed in the top end cap to measure internal gas pressure. This internal pressure is monitored throughout the run with the data-logger and on scopes at time of reaction.

The experimental configuration is shown in Figure 3, which shows the three radiant heaters used to heat the cylinder wall and the location of the Micropower Impulse Radar horns. The non-contact heaters, positioned 140 mm from the vessel wall, were chosen to reduce temperature gradients that are typically present with heater bands, and to eliminate the non-quantifiable extra confinement that heater bands provide. The three heaters are controlled by one temperature controller monitoring a RTD that is located at the center of the vessel between two of the heaters. Each end cap is heated with a separately controlled heating element. These heater elements are attached to an aluminum plate and assembly of rings that enclose the end cap and vessel flange to provide more uniform end heating conditions.

The MIR High Speed Rangefinder (HSR) is a low power, ultra-wideband radar system based on Micropower Impulse Radar (MIR) technology developed at LLNL. This radar operates by sending microwave impulses and listening for reflections off of conducting surfaces or dielectric interfaces. The current HSR sweeps out the range between the radar and the center of the experiment every 4.5 microseconds. Three radar systems are used in each experiment, with antenna pairs spaced at 120 degree intervals approximately 180 mm from the vessel wall, providing wall velocity at three angular locations. Upon receiving a trigger, digitizing scopes capture 10 ms of data centered about the trigger. We chose micropower radar for wall velocity measurement because of the long duration of these experiments and the unpredictability of the reaction time. More conventional wall velocity measurement methods using laser velocimetry are impractical due to difficulties with running a high-power laser for the several days of the experiment and then triggering the data acquisition system, in addition to problems posed by the significant heat load on the experiment from the laser. Flash radiography has been used successfully elsewhere to capture wall motion in this type of experiment – however, the resolution is poor (typically two flash images) and generally looks across only one plane of the experiment. Micropower impulse radar avoids these problems while providing a good measure of wall velocity.

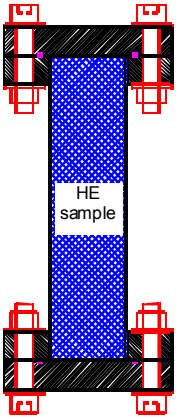

FIGURE 2. DESIGN OF STEX VESSEL.

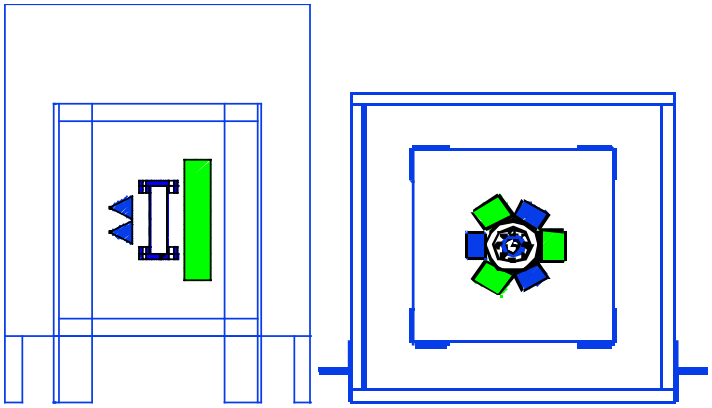

FIGURE 3. LAYOUT OF STEX EXPERIMENT, SIDE VIEW (LEFT) AND TOP VIEW (RIGHT), SHOWING RADAR HORNS AND RADIANT HEATERS. SMALL SQUARE ON RIGHT IS SHOT STAND, AND LARGE SQUARE IS SHRAPNEL SHIELD.

SAMPLE DESCRIPTION

We have studied two HMX-based explosives with the Scaled Thermal Explosion Experiment. LX-04 contains 85 wt% HMX of trimodal particle size distribution with few large particles (> 100 μm), and 15 wt% Viton A binder. PBX-9501 contains 95 wt% HMX with a trimodal particle size distribution and a significant fraction > 100 μm, with a binder of 2.5 wt% Estane and 2.5 wt% BDNPA/F. Samples for most runs were uniaxially pressed to a density of > 98.5% of theoretical maximum, although samples for runs 1, 3, 6, 7 were pressed isostatically to about the same density. The key differences between these two formulations are the proportion of HMX to binder, the inert nature of the Viton-A binder compared to the reactive Estane plasticized with energetic BDNPA/F, and the presence of larger particles in the PBX-9501.

The β→δ phase transition in HMX involves a volumetric expansion of about 6% and therefore the phase transition is hindered by high pressure.[3-7] Previously we showed that confining HMX at 200 MPa increases the phase transition temperature by over 30°C.[8] Therefore, by sizing the explosive sample so that it comes snug with the vessel wall before the phase transition, experiments with 200 MPa confinement can be conducted under conditions that prevent the phase transition. In this way, we can study the effect of HMX solid phase on thermal explosion violence. To illustrate the differences required, we compare the sample sizes for PBX-9501 in runs 8 (δ-phase) and 11 (β-phase). For run 8, the PBX-9501 was 49.66 mm diameter, 198.6 mm long, with a mass of 706 g. For run 11, the PBX-9501 was 50.69 mm diameter, 202.7 mm long, with a mass of 750 g. For each test, three cylindrical pieces of explosive were stacked to achieve the final height, with the center piece being approximately twice the length of the top and bottom piece. This was designed to ensure that the ignition point at the vertical center of the sample is not at a joint between two pieces. In all cases, a hole was drilled along the center axis of the parts to insert the internal thermocouple.

We have also studied two RDX-based explosives, Composition B and PBXN-109. The Composition B contained 63 wt% RDX, 36 wt% TNT, and 1 wt% wax. For the first two runs, the material was cast and machined into cylinders, including a hole along the axis for the internal thermocouple, each with diameter of ~49 mm and length ~68 mm. Each run contained three cylinders, with a total mass of 646 g. For subsequent experiments, the Composition B was cast into the vessel with the internal thermocouple in place, again with a total mass of 646 g. Inasmuch as the TNT melts long before the thermal explosion takes place, there was no need to maintain the accurate and costly dimensional control through casting and machining as was done for the first two runs. The PBXN-109 composition is 65 wt% RDX, 21 wt% aluminum, 7 wt% HTPB binder, and 7 wt% DOA plasticizer. The material was provided in 50 mm diameter cylindrical samples that were hand-cut to the appropriate length. The hole for the internal thermocouple was made with a hand-operated cork-boring tool.

RUN PARAMETERS

For HMX-based explosives, calculations with decomposition kinetic schemes[9] showed that a heating rate of 1°C/hr is required to locate the ignition point at the center of a 50.8mm diameter sample. At the slightly-faster rate of 1.44°C/hr, the calculated ignition point was about 10 mm from the edge. Because we expected maximum violence

with center ignited reactions, the experiments with HMX-based explosives run to date have been heated at 1°C/hr from 130°C until thermal explosion occurs, after an initial fast ramp to 130°C and 5-hour equilibration at 130°C. The top and bottom flanges are set to lag the cylinder temperature by about 5°C, to ensure that the ignition location is vertically-centered along the axis of the cylinder. The test with PBXN-109 had the same thermal profile also, whereas with Composition B, we used final ramp rates of 1, 2, and 3°C/hr.

The mass of explosive must be carefully chosen to allow for thermal expansion and any phase transitions. HMX undergoes a β→δ solid-solid phase transition about 160°C,[3-7] while the TNT component of Composition B melts at 80°C with approximately 13% increase in volume.[10] The explosive sample is sized for each experiment so that the sample comes in contact with the confinement either before, during, or after the phase transition, depending on the desired conditions for the experiment.

DATA MONITORING/LOGGING

All the collected data, from each run, is stored to a computer. This includes raw data and data that have been corrected to calibration standards and adjusted to engineering units. These data include: temperatures of the 12 RTDs attached to the outside of the vessel wall, the five internal TCs located every 50.8mm down the center of the vessel tube, internal vessel gas pressure, the three controlling RTDs that control the lamps and two end heaters, and the four strain gauges, which record axial and hoop strain. This data is recorded approximately every 45 seconds. For several hours prior to the reaction, we record the five internal thermocouple temperature data at a rate of approximately every second. At time of reaction, as detected by a trigger system, we record runaway strain from the four strain gauges and the internal vessel gas pressure from the transducer, with a time resolution of about one microsecond.

For each Scaled Thermal Explosion Experiment we compile an extensive data package, containing: Shot Run Summary with a brief detail of the entire run; Assembly Log with details of identification of vessel, end caps and internal TC used on the assembly, rate of rise during a seal leak check and weight and dimensions of material used; Material information on machining dimensions of pellets, formulations, safety data and thermal expansion; Ramp Rate worksheet listing the ramp rates and soak times throughout the run; Run Log that documents details throughout the run; Fragment Collection Location sheet that shows the location of collected fragments in the firing tank; Fragment Collection Worksheet listing fragment weight, approximate size and fragment condition; Result Details qualitatively describing overall damage to the experimental hardware; Radar Results showing detailed data from the MIR; Digital photos taken throughout the assembly, set-up, and disassembly of the experiment; standard analog (30 fps) and high speed digital (up to 20,000 fps) video recording; and the temperature, strain and pressure data discussed in the previous paragraph.

RELATING REACTION VIOLENCE TO DETONATION

To relate the wall velocity measurements to detonation energy, we turn to the Gurney method. In this approach, for a metal cylinder being expanded by a detonating explosive, the wall velocity can be estimated from the test geometry and a "Gurney energy" that is characteristic of the explosive.[11]

$$V_{wall} = \sqrt{2E}\left(M/C + 1/2\right)^{-1/2} \quad (1)$$

where:

$$M/C = \left[\left(OD/ID\right)^2 - 1\right]\rho_m/\rho_c \quad (2)$$

The quantity $\sqrt{2E}$ is the "Gurney energy", OD and ID are the outer and inner diameter of the metal cylinder, ρ_m is the density of the cylinder wall, and ρ_c is the density of the explosive filling the cylinder. The Gurney energy is tabulated for many explosives undergoing detonation.[11]

Using the wall velocity from the thermal explosion and the test geometry, we can rearrange Eqs.(1) and (2) to calculate a thermal "Gurney energy" $\sqrt{2E_{thermal}}$ for each experiment. We then estimate the percent of detonation energy represented by the thermal explosion by:

$$\%\ \text{of det. energy} = \left(\sqrt{2E_{thermal}}/\sqrt{2E}\right)^2 \times 100 \quad (3)$$

This quantity is shown in Tables 1 and 2 for HMX-based explosives and for RDX-based explosives, respectively. The quantity "average" wall velocity is calculated using the formula:

$$\text{"average" wall vel.} = \text{mean vel.}\Big/\left(1 + \frac{\text{std dev vel.}}{\text{mean vel.}}\right) \quad (4)$$

which reduces the effect of one very high velocity reading on the overall average. If one radar channel records very high velocity while the others do not, the reaction is most likely not very violent, and Eq.(4) was developed on this basis.

RESULTS WITH HMX-BASED EXPLOSIVES

The results for LX-04 and PBX-9501 are summarized in Table 1. Details of the thermal explosion progression

may be seen in the internal temperature data preceding and during the thermal explosion. Typical results are shown in Figures 4 and 5 for PBX-9501 (run 27, see Table 1). In Figure 4, the internal temperature data at the middle of the sample shows that slow self-heating had begun even before the clearly-visible endothermic phase transition at 160-164°C. Following the phase transition, slow self-heating resumed and is visible in the upper and lower internal thermocouples as well; eventually the self-heating accelerated to a runaway condition.

The thermal excursion during the explosion is recorded by using a fast scan rate, with all five internal temperatures recorded each second. (The time response of the internal thermocouple, with a wall thickness of 0.41 mm, is sufficiently slow so that a one-second recording period is appropriate.) As shown in Figures 4 and 5, the temperature at the middle is the highest prior to the onset of rapid reaction. However, as the runaway accelerates the location of the highest temperature sometimes shifts. In Run 27, shown in Figure 5, the reaction moved upward in the vessel, with thermocouples above the middle showing higher temperatures. In other runs, we have seen the reaction move downward. The samples are made as uniformly as is possible, but apparently there is still sufficient inhomogeneity to drive the reaction in different directions in different tests. This effect will be very difficult to capture in computer simulations of thermal explosions. We note that the reaction associated with the data in Figure 5 was so mild that the internal thermocouples survived the explosion and continued to report temperatures.

TABLE 1. SUMMARY OF SCALED THERMAL EXPLOSION EXPERIMENTS WITH HMX-BASED EXPLOSIVES. ALL ARE 50.8 MM DIAMETER, 203 MM LENGTH, WITH A RAMP RATE OF 1°C/HR ABOVE 130°C. ONSET TEMPERATURE IS THE HIGHEST READING ON THE VESSEL EXTERIOR AT THE TIME OF RUNAWAY REACTION. SOME VESSELS WERE VENTED PRIOR TO THERMAL EXPLOSION, AS SHOWN BY STRAIN GAUGE AND TEMPERATURE DATA AND BY VISUAL AND AURAL OBSERVATION. VIOLENCE IS INDICATED BY FRAGMENT DISTRIBUTION, BY PEAK WALL VELOCITIES MEASURED BY RADAR, BY CALCULATION OF PERCENT OF DETONATION ENERGY, AND BY FINAL STRAIN RATE.

Test #	Expl-osiv	Confinement, MPa	HMX phase	Onset temp., °C	Vented?	Fragments[†]	Wall velocity 3 channels), m/s	"Average" wall velocity, m/s[†††]	% of detonation energy	Log (radial strain rate, s^{-1})
1	LX-04	25[*]	δ	173	No	None	13, 0, 0	2	0	-
3	"	50	δ	172	No	None	0, 0, 40	5	0	-
6	"	200	δ	192	Yes	4L, 4S	800, 200, 400	280	2	3.5
28	"	200	δ	191	Yes	None	-90, 850, 130	110	0	1.7
9	"	200	δ	192	No	None	0, 800, 0	98	0	-
29	"	200	δ	191	No	None	0, 1100, 450	250	2	1.7
7	"	200	β	187	Yes	1 S	70, 0, 1000	140	0	2.1
10	"	200	β	188	No	None[**]	200, 200, 200	200	1	4.1
2	PBX-9501	50	δ	170	No	None[††]	130, 60[***], 130	77	0	-
27	"	50	δ	170	No	None[††]	700, 700, 700	700	5	-
4	"	200	δ	169	Yes	5 L, 9 S	600, 800, 200	340	3	-
8	"	200	δ	170	No	6 L, 10 S	300, 800, 700	420	4	-
5	"	200	β	169	Yes	"Detonation"	1700, 1600, 1900	1600	57	4.1
11	"	200	β	165	No	"Detonation"	1400, 1700, 1200	1200	33	4.3

* vessel was 50 MPa design, but flaw in metal led to failure at lower pressure.

[†] none – vessel split open; L: large fragments 50 mm and above; S: small fragments ~ 25mm; "detonation" – vessel destroyed, hole punched in end cap, nothing recoverable from cylinder wall

[**] Bottom heater failed during run. Reaction initiated above center of vessel, which split into three vertical segments aligned with three radiant heaters.

[††] vessel completely split and folded back onto itself.

[***] radar 2 recorded motion ~ 2ms later than radar 1 & 3, as the vessel walls folded back into view of radar 2.

[†††] "ave" wall velocity = mean V / (1+std. dev. V / mean V), calculated from three radar velocities.

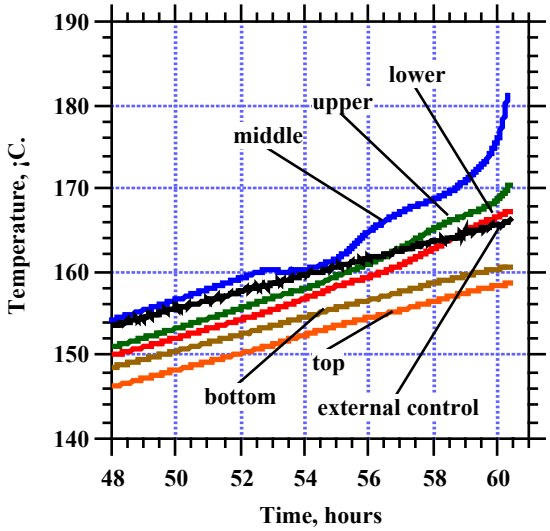

FIGURE 4. RUN 27, PBX-9501: INTERNAL TEMPERATURES AND EXTERNAL CONTROL TEMPERATURE IN FINAL HOURS PRECEDING THERMAL EXPLOSION.

In many experiments we successfully recorded axial and radial strain during the thermal explosion. The radial strain rate data during the final wall expansion just prior to loss of signal are reported in Table 1 and displayed in Figure 6 compared with the "average wall velocity". In this figure we see that data set for each explosive shows reasonable correlation, but the data sets together show much less correlation. There is uncertainty in both the wall velocity and strain rate results, and we are just beginning to study and understand their correspondence. Also, the strain rate data are preliminary at this point, and further analysis may provide refined values.

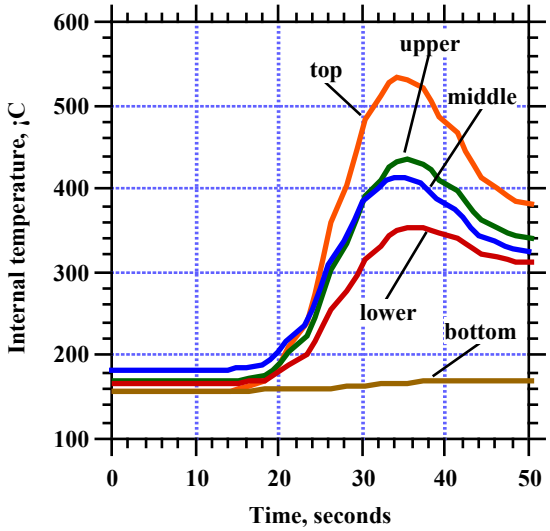

FIGURE 5. RUN 27, PBX-9501: INTERNAL TEMPERATURES DURING THERMAL RUNAWAY AND EXPLOSION.

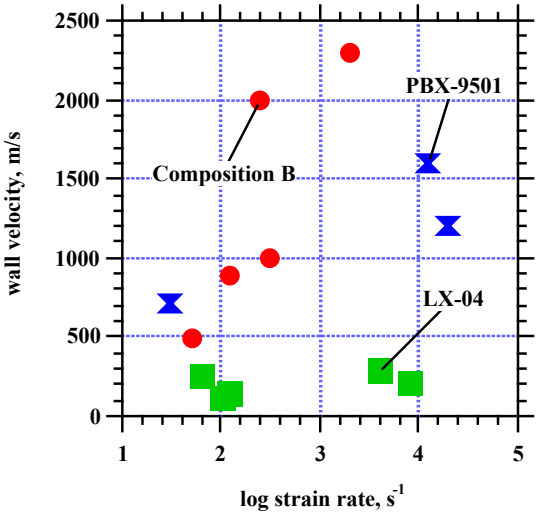

FIGURE 6. COMPARISON OF "AVERAGE" WALL VELOCITY WITH RADIAL WALL STRAIN RATE.

We can draw some observations from the entire data set with HMX explosives. Composition is very significant, since LX-04 (with 15% binder) produces thermal explosions that are consistently less violent than those with PBX-9501 (2.5% binder, 2.5% plasticizer). With LX-04 the maximum percentage of detonation energy is 2% , while with PBX-9501 this is as high as 57%. Effects of confinement are as expected, with higher confinement leading to more violent reactions in both LX-04 and PBX-9501.

The effect of the HMX phase transition is complex. For experiments at low confinement, the phase transition takes place and the reaction involves δ-phase HMX. As discussed above, the phase transition temperature is increased by about 30°C at pressures of 30,000 psi (200 MPa), and therefore the phase transition may be retarded by sizing the sample to come snug with the confinement prior to reaching the phase transition temperature. In this latter case, the confining pressure increases the phase transition temperature sufficiently high that the thermal explosion occurs before the phase transition. The internal thermocouple gives a clear endotherm indicative of the phase transition in the former case with δ-phase, as seen in Figure 4, whereas no such feature is seen in the latter case with β-phase. Each experiment in Table 1 is labeled with the final HMX phase prior to thermal explosion.

For LX-04, there is no strong effect of HMX phase, with the violence being about the same for the two phases.

We do note that the onset temperature with LX-04 is reduced about 3°C when the phase transition is retarded. For PBX-9501, the effect of HMX phase is profound. In addition to a lowering of the onset temperature of 1-4°C, the nature of the thermal explosion changes completely when the phase transition is retarded. The violence appearing essentially "detonative" with very high wall velocities, holes punched in inch-thick end caps, and complete destruction of the confining cylinder and surrounding diagnostics. For the two replicate runs at this condition, the percentage of detonation energy is quite high, 33-57%. These two runs were the only ones in which a very high degree of violence was seen with HMX-based explosives.

The results in Table 1 are complicated by the fact that some of the experiments were vented, allowing decomposition gases to escape during the heating process. Each run in Table 1 is labeled accordingly. Of the runs labeled as vented, all but runs 7 and 28 were vented when the internal thermocouple leaked at the top, allowing gas from the top center of the sample to escape through the thermocouple sheath. Run 28, on the other hand, was deliberately vented by eliminating the gasket sealing the top flange, allowing gas to escape from the top outer edge of the explosive. This difference in location of the leak apparently proved to be significant, with leakage from the center leading to higher violence with LX-04 (compare run 6 with center leakage and run 28 with edge leakage). Although initially unexpected, this behavior is consistent with modeling results by Larry Luck at Los Alamos National Laboratory, in which he showed that thermal explosion reactions would be expected to be different for cases where gas took different pathways out of the solid.[12] We note that the data from run 7 did not conclusively show where the leak occurred.

The effects of venting are apparent in the internal thermocouple records. Thermal explosion is preceded by a period where the interior of the explosive undergoes self-heating as the exothermic reaction accelerates. The onset of self heating is shown in Figure 7 for the runs at 200 MPa confinement. We can make several observations from this plot. Overall, PBX-9501 begins to self-heat at a lower temperature than LX-04. The endothermic β→δ phase change is clearly visible in the runs with LX-04 in δ phase, and is not seen in the runs with β phase HMX; the same is true for the runs with PBX-9501. For LX-04, the runs with β phase HMX reacted at lower external temperatures than with δ phase HMX, although this was not the case for PBX-9501. Finally, in all cases the runs where the seal was maintained showed self-heating of a shorter duration in comparison to the same conditions but vented. The most dramatic case was for PBX-9501 in the β phase, where in the sealed experiment there was very little self heating before explosion. This may be explained by the loss of gaseous intermediates and products in the vented case; energy is removed from the system both in the latent heat and the chemical energy in incompletely reacted species. The chemistry of the thermal explosion is therefore somewhat different in the vented and sealed cases.

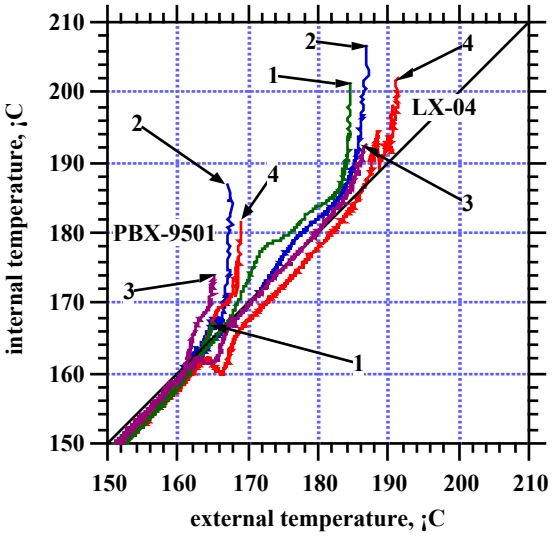

FIGURE 7. SELF-HEATING DATA FOR EACH RUN AT 200 MPA CONFINEMENT. ARROWS POINT TO END OF DATA, AT WHICH POINT EXPLOSION OCCURRED. KEY: 1 – β-PHASE, SEALED; 2 – β-PHASE, VENTED; 3 – δ--PHASE, SEALED; 4 – δ--PHASE, VENTED

Regardless of the actual reason, we conclude that gas release through venting leads to higher internal temperatures and, in some cases, more violent thermal explosions. This is counter to intuition saying that venting should lead to less violent reactions.

The quantity reported as the "% of detonation energy" is very low for all experiments with HMX-based explosives, except for the two runs with PBX-9501 under high confinement and with samples sized to maintain the HMX in β-phase. There is clearly a significant difference between the reaction in the latter two runs and those in the other runs with HMX. Our hypothesis is that the phase of the HMX is the difference, and we are continuing efforts to demonstrate (or disprove) this through measurement of the phase present under both types of conditions.

RESULTS WITH RDX-BASED EXPLOSIVES

With RDX-based explosives, PBXN-109 gave a very mild thermal explosion. In contrast, thermal explosions with Composition B were quite violent. As shown in Table 2, the energy release appeared detonative in two cases with Composition B, was quite high in most of the other experiments with Composition B, and was very mild with PBXN-109. Only with relatively low confinement and a relatively high thermal ramp rate was the violence from Composition B as low as was seen in most of the HMX ex-

periments. This is consistent with anecdotal evidence from DoD colleagues, who report that Composition B gives very violent thermal explosions.

The effects of confinement and thermal ramp rate for Composition B are shown in the data in Table 2. At the lowest thermal ramp rate of 1°C/hr, the reaction was essentially detonative regardless of confinement, but at the faster rate of 3°C/hr the lower confinement led to lower reaction violence, as expected. For both confinement conditions, faster thermal ramp rates led to lower violence, although the effect was not entirely consistent.

The behavior of Comp B is made more complex by the fact that the TNT is molten for a long time before the thermal explosion takes place. This gives rise to many possible mechanistic effects. First, the material has no strength and any physical impetus may give rise to increased surface area for deflagration reactions to operate on. In addition, the formation of bubbles in the molten TNT could lead to sensitization. The presence of the molten TNT also allows for thermally-driven convective heat transfer to occur within the explosive, which would heat a larger fraction of the material to higher temperatures when compared to explosives in which only solid-state heat conduction is active. With more material hot, more material could participate in the initial thermal explosion reaction steps and therefore lead to higher violence of reaction. Finally, RDX is somewhat soluble in molten TNT and the melting point of RDX is probably lowered by formation of a eutectic mixture. A possible indication of this latter point is shown in Figure 8, in which the internal temperature data for the last several hours of Run 18 are shown. In addition to the self-heating that is particularly evident in the middle and upper internal thermocouples, there is an endothermic signal at the upper thermocouple around 195°C. There are two rapid decreases and subsequent rapid increases in temperature, such as might be expected if RDX crystals near the thermocouple melted. While this hypothesis remains somewhat conjectural at this time, it seems likely that the presence of molten TNT changes the RDX chemistry, perhaps significantly.

TABLE 2. SUMMARY OF RESULTS OF SCALED THERMAL EXPLOSION EXPERIMENTS WITH RDX-BASED EXPLOSIVES. FOR ALL: 50.8 MM DIAMETER, 203 MM LENGTH; RAMP RATE ABOVE 130°C IS SHOWN. ONSET TEMPERATURE IS THE HIGHEST READING ON THE VESSEL EXTERIOR AT THE TIME OF RUNAWAY REACTION. ALL VESSELS WERE SEALED, WITH NO VISUAL OR AUDIBLE EVIDENCE OF VENTING. VIOLENCE IS INDICATED BY FRAGMENT DISTRIBUTION, BY PEAK WALL VELOCITIES MEASURED BY RADAR AND BY CALCULATION OF PERCENT OF DETONATION ENERGY.

Tes #	xpl-osiv	Confine ment, MPa	Ramp rate, °C/hr	Onset emp. °(	Frag-ments*	Wall velocity † 3 channels), m/s	"Average" all velocit m/s **	% of det nation en ergy	Log (radial train rate, s $^{-1}$)
12	Comp B	200	1.0	159	37S	2100, 2000,	2000	100	2.0
13	"	200	1.0	160	52S	2000, 2800, 1000	1300	45	-
17	"	200	2.0	164	48S	, 1800, 600	700	13	2.5
18	"	200	3.0	166	48S	1100, 900,	880	20	1.7
19	"	100	1.0	164	22S	2500, 2500,	2500	100	2.7
20	"	100	3.0	169	1S††	200, ,	200	1	1.7
36	PBXN-109	200	1.0	152	3L††	250, , 180	180	1	2.6

* S: small fragments ~ 25mm; L: large fragments 50 mm and above

† in some cases, radar channel did not report. Missing data are shown by inserted commas.

** "ave" wall velocity = mean V / (1+std. dev. V / mean V), calculated from three radar velocities.

†† vessel wall was largely intact, but greatly deformed, with the few fragments shown.

PBXN-109, on the other hand, was quite mild in its explosive response. As shown in Table 2, the wall remained largely intact, with three large fragments at modest velocities. The explosion was followed by extensive combustion of PBXN-109 that was not consumed in the explosion. The internal temperature data, shown in Figure 9, show thermal runaway at a lower temperature than Composition B. In addition, the internal temperatures in Figure 9 are quite smooth, with no endotherms or other irregularities as are seen with Composition B in Figure 8. This demonstrates the importance of the binder physical and chemical properties on the overall thermal behavior. The energetic

liquid TNT in Composition B leads to a much more complex thermal history and, presumably, more complex reaction mechanism than the fairly unreactive HTPB and aluminum in PBXN-109.

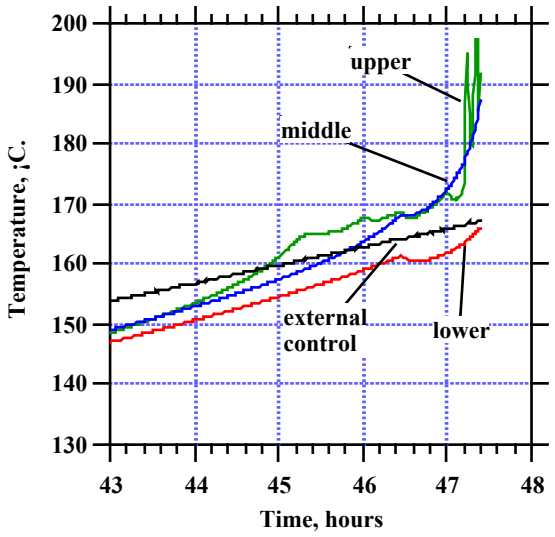

FIGURE 8. INTERNAL TEMPERATURE DATA FROM RUN 18 WITH COMPOSITION B, SHOWING SELF-HEATING AND ENDOTHERM AT UPPER THERMOCOUPLE PRIOR TO IGNITION.

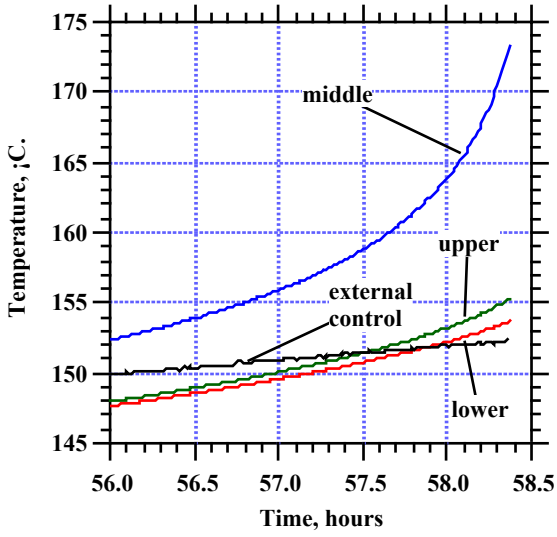

FIGURE 9. INTERNAL TEMPERATURE DATA FROM RUN 36 WITH PBXN-109, SHOWING SELF HEATING.

OVERALL REACTION VIOLENCE

The overall picture of reaction violence from each experiment must be drawn from consideration of all the diagnostics. It is possible for one diagnostic to record an apparently very violent event, such as if one fragment is ejected directly towards a radar detector or if a strain gauge happens to be located very close to the failure point of the metal wall. Only by having several types of measurements and comparing them can we draw a consistent picture of reaction violence across a set of experiments. The data perhaps most useful to those developing or validating predictive models of thermal explosion are the strain rate in the vessel wall, with wall velocity being somewhat more difficult to interpret and fragmentation data being very difficult because of the not-well-understood nature of metal fracture under these conditions of fairly low strain rates. However, any strain rate data from this or other thermal explosion experiments must be considered against the integrated picture of reaction violence, to ensure that the strain rate data truly represent the behavior of the entire assembly and are not distorted by their sampling of a very specific location on the vessel wall. If all available data for a particular experiment are consistent, we may use them to quantify the reaction violence. If the data are not consistent, then judgement must be applied in assigning a quantification to reaction violence.

CONCLUSIONS

The Scaled Thermal Explosion Experiment, with carefully defined and controlled initial and boundary conditions and extensive diagnostics, is providing detailed information on thermal explosion violence and on the processes leading to the eventual thermal explosion. Clear differences can be seen between formulations containing the same explosive component, such as HMX-based LX-04 and PBX-9501; these differences must be considered in analysis of hazards engendered by systems containing these or related explosives. Comparing RDX-based formulations, the very high violence from Composition B thermal explosions under many conditions contrasts with the very low violence from PBXN-109, highlighting the effect of composition on the overall thermal response.

Each experiment generates a large data set including temperatures, strains, and wall velocities, as well as photographs and videos of the experiment set up, execution, and aftermath. If the reader is interested in getting any or all of the data sets, he may contact the second author.

The Scaled Thermal Explosion Experiment was designed with modeling in mind, both in the simplicity and thorough definition of the design and in the provision of extensive diagnostics. The temperature, wall velocity, and strain rate diagnostics provide data necessary to develop

and validate predictive computational models such as is being done by Nichols and coworkers.[1]

ACKNOWLEDGEMENTS

Support for this work was provided by the LLNL Energetic Materials Surety Program and by the DoD Office of Munitions through the DoD/DOE Memorandum of Understanding.

We would like to thank the following people for their contributions: Jack Reaugh, Al Nichols, Craig Tarver, LeRoy Green, Ed Lee, Matt McClelland, and Tri Tran for help in the conceptual design, development, and interpretation of results from the STEX test; Greg Sykora, Les Calloway, Kevin Black and Dan Greenwood for electronic support; Kou Moua and Ed Silva for mechanical and fabrication support; Doug Poland, Bob Simpson, and Tom Rosenbury for micropower impulse radar measurements; Denise Grimsley, Bill Gilliam and Larry Crouch in supporting execution of these experiments in the High Explosives Applications Facility at LLNL. We thank Alice Atwood and Pat Curran at NAWC China Lake for providing the PBXN-109 samples.

This work was performed under the auspices of the U.S. Department of Energy by the Lawrence Livermore National Laboratory under contract number W-7405-Eng-48.

REFERENCES

1. A.L. Nichols, III, A. Anderson, R. Neely and B. Wallin, "A Model for High Explosives Cookoff", in *Proceedings of 12th International Detonation Symposium*, San Diego, CA, Office of Naval Research, p. (2002).

2. J.L. Maienschein, J.F. Wardell, R.K. Weese and B.J. Cunningham, "Understanding and Predicting the Thermal Explosion Violence of HMX-Based and RDX-Based Explosives - Experimental Measurements of Material Properties and Reaction Violence", in *Proceedings of 12th International Detonation Symposium*, San Diego, CA, Office of Naval Research, p. (2002).

3. H.H. Cady, "Studies on the Polymorphs of HMX", Los Alamos Scientific Laboratory, LAMS-2652 (October 18, 1961).

4. W.C. McCrone, "Crystallographic Data: Cyclotetramethylene Tetranitramine (HMX)", *Analytical Chem.*, **22**, 1225 (1950).

5. A.S. Teetsov and W.C. McCrone, "The Microscopial Study of Polymorph Stability Diagrams", *Microscop. Cryst. Front.*, **15**, 13 (1965).

6. M. Herrmann, W. Engel and N. Eisenreich, "Phase Transitions of HMX and their Significance for the Sensitivity of Explosives", in *Proceedings of the Technical Meeting of Specialists MWDDEA AF-71-F/G-7304 - Physics of Explosives*, p. 12 (1990).

7. R.E. Cobbledick and R.W.H. Small, "The Crystal Structure of the δ-form of 1, 3, 5, 6 - Tetranitro-1, 3, 5, 7-tetraazacyclooctane (δ-HMX)", *Acta Cryst.*, **B30**, 1918 (1974).

8. J.L. Maienschein and A.L.Nichols III, "Ignition and Initiation Phenonema: Cookoff Violence Prediction", in *Joint DoD/DOE Munitions Technology Development Program FY-99 Progress Report*, pp. II-69 - II-103, Lawrence Livermore National Laboratory, UCRL-ID-103482-99 (May 31, 2000).

9. R.R. McGuire and C.M. Tarver, "Chemical Decomposition Models for the Thermal Explosion of Confined HMX, TATB, RDX,and TNT Explosives", in *Proceedings, Seventh Symposium (International) on Detonation*, Annapolis, MD, Naval Surface Weapons Center, p. 56 (1981).

10. J. Köhler and R. Meyer, *Explosives, Fourth, revised and extended edition*, VCG, Weinham (1993).

11. B.M. Dobratz and P.C. Crawford, "LLNL Explosives Handbook: Properties of Chemical Explosives and Explosive Simulants", Lawrence Livermore National Laboratory, UCRL-52997 change 2 (January 31, 1985).

12. L. Luck, Los Alamos National Laboratory, personal communication, October 2001.